Properties of fluorescence based on the immobilization of graphene oxide quantum dots in nanostructured porous silicon films

Lei He (蕾 何)[1,*], Zhenhong Jia (贾振红)[2], and Jun Zhou (周 骏)[3]

[1]*School of Physical Science and Technology, Xinjiang University, Urumqi 830046, China*
[2]*School of Information Science and Engineering, Xinjiang University, Urumqi 830046, China*
[3]*Department of Physics, Ningbo University, Ningbo 315211, China*
**Corresponding author: helei523@163.com*

Received October 22, 2015; accepted January 25, 2016; posted online March 28, 2016

The fluorescence of graphene oxide quantum dots (GOQDs) that are infiltrated into porous silicon (PSi) is investigated. By dropping activated GOQDs solution onto silanized PSi samples, GOQDs are successfully infiltrated into a PSi device. The results indicate that the intensity of the fluorescence of the GOQD-infiltrated multilayer with a high reflection band located at its fluorescence spectra scope is approximately double that of the single layer sample. This indicates that the multilayer GOQD-infiltrated PSi substrate is a suitable material for the preparation of sensitive photoluminescence biosensors.

OCIS codes: 050.5298, 120.5700, 130.3990, 160.2540, 160.4760.
doi: 10.3788/COL201614.041601.

Nanometer-sized graphene oxide particles, known as graphene oxide quantum dots (GOQDs), exhibit promising photoluminescence and optoelectronic properties[1–10] because of their strong quantum confinement and edge effects[11–21]. This makes them an exciting new type of fluorescent material with a graphene structure[22]. GOQDs have many outstanding properties, including chemical inertness, excellent biocompatibility, resistance to photo bleaching, and ease of production, among others[23,24]. In the biomedical field, GOQDs have been used as fluorescent tags in biomarkers and fluorescent probes in biomolecule detection[25]. Porous silicon (PSi) is a material with a large internal surface area, good biocompatibility, ease of functionalization, size-selective filtering capabilities, and the capacity to fabricate various types of photonic devices with different structures[26,27]. Because of these qualities, PSi has attracted great interest in the field of biosensing[28–30]. The luminescence properties of PSi devices can be improved by embedding quantum dots (QDs) into PSi with photonic crystal structures[31,32]. Liu *et al.* embedded CdSe QDs into PSi Bragg and microcavities, which successfully enhanced the fluorescence intensity of CdSe QDs[33,34]. Though some researchers have investigated the process of embedding graphene oxide fragments into PSi in order to produce a fluorescent signal[35], there has not yet been research about improving the photoluminescence properties of GOQDs by adding them to PSi structures.

In this work, the enhancement of GOQDs' photoluminescence by PSi photonic crystal structures is reported. GOQDs were successfully infiltrated into a PSi device. Additionally, an appropriate multilayer PSi device was fabricated, and its high reflection band covered the fluorescence spectra of GOQDs. Then, any changes in the photoluminescence intensity were observed.

The GOQDs was purchased from Nanjing XFNANO Materials Technology. The size distribution of the GOQDs is presented in Fig. 1(a), and their photoluminescence spectra are shown in Fig. 1(b).

The PSi substrate was fabricated using a p-type Si (resistivity 0.03–0.06 Ωcm, ⟨100⟩ orientation). Before

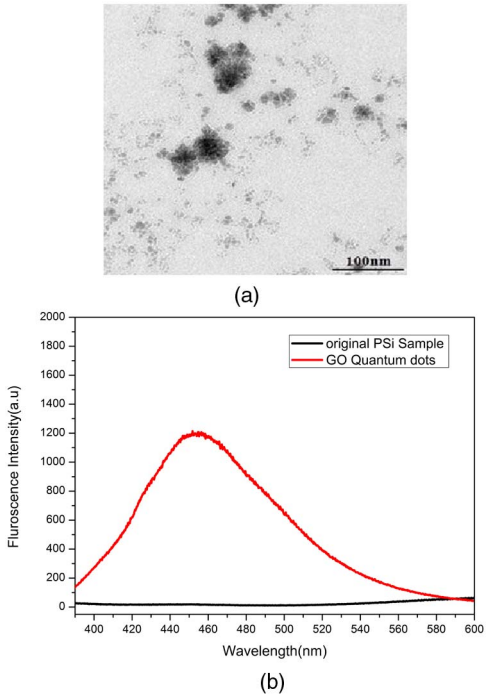

Fig. 1. (a) SEM image of QDs used in the research. (b) Photoluminescence spectra of QDs (0.5 mg/mL) and original PSi sample at an excitation wavelength of 370 nm.

electrochemical anodization, all of the pieces were cleaned with solutions of carbinol, alcohol, and deionized water in succession. PSi substrates were fabricated by electrochemical etching in an electrolyte ($HF:CH_3CH_2OH$, 1:1 in volume). The electrochemical etching parameters were manipulated in order to obtain samples of periodically changing porosity or refractive index. The PSi Bragg reflector is a bandgap area with high reflectivity. PSi Bragg reflectors with different bandgap locations were prepared by controlling the electrochemical etching time and electric current density parameters according to

$$m\lambda_{\text{bragg}} = 2(n_L d_L + n_H d_H), \tag{1}$$

where m is an integer, n_L (n_H) and d_L (d_H) are the low (high) refractive index and thickness of the PSi layers, respectively, and λ_{Bragg} is the center of the bandgap. A mutilayer PSi device with a bandgap center at 450 nm was produced because this high reflection band coincided with the QDs' fluorescence emission spectra, resulting in the enhancement of the sample's fluorescence. For comparison, another PSi Bragg reflector was produced with a high reflection that was far beyond the fluorescence emission of the GOQDs.

Three samples were used for the experiments. The first sample's bandgap center was at 450 nm after it was infiltrated with GOQDs. This bandgap area almost covered the GOQDs' fluorescence emission spectra. The sample consisted of two parts: a single layer section, and a distributed Bragg reflection (DBR) multilayer section. The single-layer PSi was fabricated with a current density of 105 mA/cm^2 for 4 s, while the 12 periodic DBR structures were fabricated via an alternating current density of I_H= 100 mA cm^{-2} and I_L=20 mA cm^{-2}. The etching time of each layer was 1 and 1.5 s.

The second sample's bandgap center was at 530 nm after it was infiltrated with GOQDs, which is out of the QDs' fluorescence emission spectra. Otherwise, the structure is identical to the first sample, with the exception of the electrochemical etching parameters of the Bragg reflector, which were as follows: $I_H = 100$ mA cm^{-2} and $I_L = 20$ mA cm^{-2}. The etching time of each layer was 1.2 and 1.8 s.

For a reasonable comparison, the third sample was a single-layer PSi. The etching conditions of this sample were identical to the single layer of the first sample.

After being etched, the substrates were cleaned with deionized water and air dried at room temperature. Then, all of the samples were oxidized in hydrogen peroxide (30%) at 80°C for 3 h. Then, the oxidized PSi samples were immersed in a 5% solution of (3-aminopropyl) triethoxysilane (APTES) in water/methanolmixture (v/v.1:1) for 1 h at room temperature in order to successfully attach the GOQDs to the PSi wall. After the reaction time was complete, the sample was washed in toluene in order to remove any redundant APTES. The sample was then baked at 100°C for 10 min.

The surface of graphene oxide has many oxygen-containing groups, such as carboxyl and epoxy groups. This carboxyl can be reacted with NH_2-SiO_2 on the PS surface, allowing the GOQDs to successfully attach to the PSi surface. Therefore, 0.002 g N-(3-Dimethylaminopropyl)-N'-ethylcarbodiimide hydrochloride (EDC) was added to a 10 mL graphene oxide (1 mg mL^{-1}) solution. The resulting product was then mixed for 30 min with magnetic stirring at room temperature to activate the carboxyl. Subsequently, the equal activated GOQD solution was allowed to trickle over the silanized PSi samples for 6 h at room temperature. The GOQDs aggregated slowly onto it. The sample was then washed in methyl alcohol in order to remove any redundant QDs on the surface. Finally, the PSi samples were allowed to air dry.

The spectrum of reflection and photoluminescence was detected by a spectrophotometer (Hitachi U-4100, Japan) and a fluorescence spectrophotometer (Hitachi F-4600, Japan), respectively. The excitation wavelength was 370 nm. The morphology of the PSi Bragg reflectors was detected by a ZEISS SUPRA55 VP scanning electronic microscope (SEM).

Figure 2 shows a top-view and cross-sectional view SEM image of the PSi Bragg reflector (sample 1). The dark-colored PSi layers were formed by etching with a current density of 100 mA cm^{-2}, and the light-colored layers were etched by a current of 20 mA cm^{-2}.

The fact that the GOQDs infiltrated into the PSi was evidenced by the reflectance spectrum (Fig. 3) and the fluorescence spectrum (Fig. 4). In addition, an energy-dispersive spectrometer was used to measure the carbon content in the PSi sample, and the results of that analysis are shown in Table 1. This figure shows that the

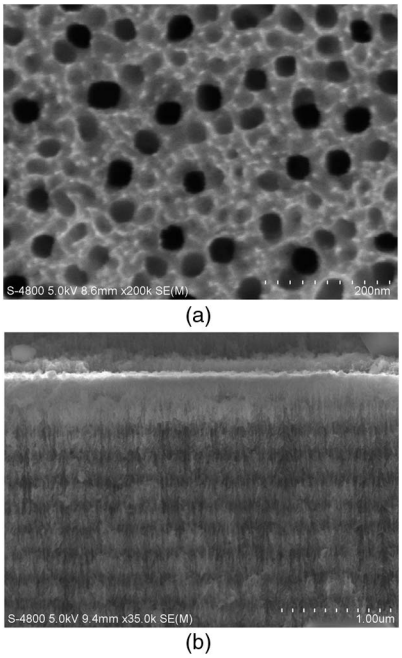

Fig. 2. Top-view and cross-sectional view SEM images of PSi sample.

Table 1. Element Content Table of the Doped PSi Sample by Energy-Dispersive Spectrometer

Spectrogram	State	C	O	Si	Total	
1	on	17.04	24.76	58.20	100.00	(According to the weight percentage)
2	on	15.21	22.99	61.80	100.00	
Average		16.12	23.88	60.00	100.00	
Standard deviation		1.29	1.25	2.54		
Maximum		17.04	24.76	61.80		
15.21		22.99	58.20			

percentage of carbon was about 16.12%. These figures prove that the GOQDs successfully coupled to the PSi surface. As shown in Fig. 3, the reflection spectrum of the PSi Bragg reflector red-shifted about 20 nm after the GOQDs were doped. This is because the GOQDs were deposited on the pore wall of PSi and increased the effective refractive index.

In order to investigate the influence of Bragg mirrors with different reflection bands on the fluorescence intensity, two different types of mutilayer PSi devices were prepared in this work. As shown in Fig. 5, their bandgaps are different. The location of one type (sample 1) coincided with the fluorescence emission peek, while the other (sample 2) was far beyond this peak. By comparing their fluorescence spectra with the single-layer sample (Fig. 6), an obvious enhancement in the fluorescence intensity of sample 1 was detected. However, sample 2 showed no enhancement in fluorescence, and, in fact, its fluorescence intensity was not as good as the single-layer sample. The excitation wavelength that was used was 370 nm, which is located outside the bandgap of the multilayer

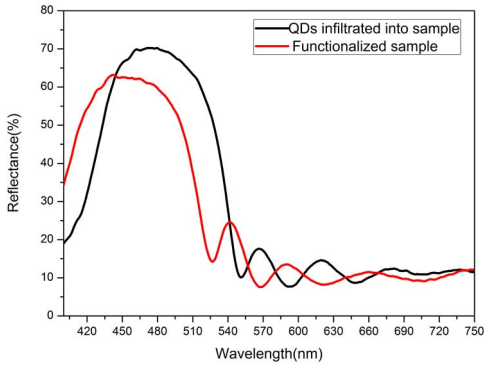

Fig. 3. Red shift of multilayer PSi sample after the infiltration of QDs.

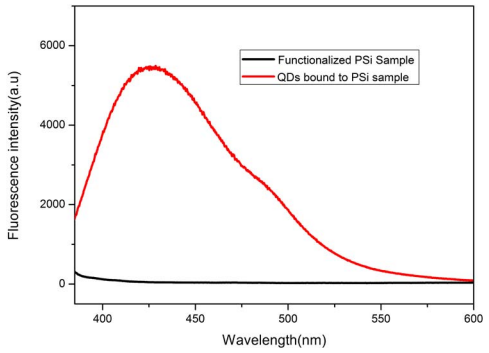

Fig. 4. Fluorescence intensity of the above PSi sample with or without QDs coupled.

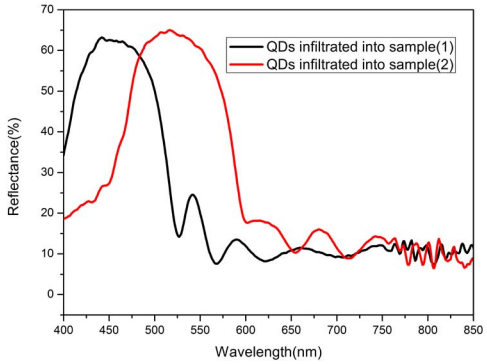

Fig. 5. Reflectance spectra of two types of PSi devices after coupling with GOQDs' (sample 1) high reflection band coinciding with the fluorescence emission spectra. In sample 2, the high reflection band was far beyond the fluorescence emission spectra of the GOQDs.

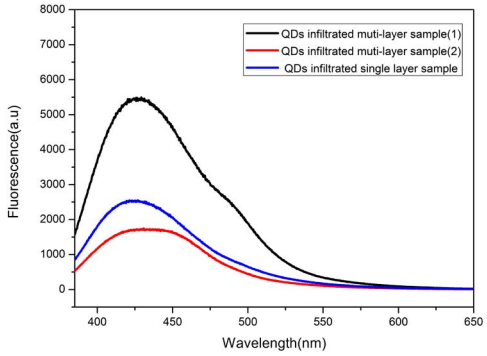

Fig. 6. Fluorescence emission spectrum of the infiltrated PSi sample: fluorescence of the mutilayer sample (1), whose high reflectance band is located at fluorescence (black line), fluorescence of mutilayer sample (2), whose high reflectance was beyond the fluorescence emission spectra (red line), and the fluorescence of the single-layer sample (blue line).

PSi, causing the reflectivity coefficient to be lower, while the transmission coefficient of the excitation light inside the multilayer PSi was higher. Meanwhile, the fluorescence of the GOQDs emission spectrum was located at 440 nm, which is in the bandgap of the multilayer PSi (sample 1). Therefore, the structures prevented the upward and downward fluorescence from transmitting inside the PSi and reflected the light to the surface of the PSi so that the fluorescence of the sample was enhanced. In addition, it was found that the GOQDs' fluorescence emission spectra blue-shifted after the infiltration. We think the reason is that QDs' energy levels interacts with the PSi surface state levels so that a series of new energy levels are formed after infiltration.

A special mutilayer PSi device is fabricated as an efficient fluorescence enhancement substrate with potential applications in the biomedical field. GOQDs are successfully infiltrated into PSi. A comparison of the fluorescence intensities of the GOQDs that are infiltrated into single-layer and multilayer PSis reveals that the location of the high reflection band of PSi has a significant effect on the enhancement of the fluorescence in the resulting samples. Only the multilayer PSi sample with a high reflection band that falls into the fluorescence peak scope is found to have a fluorescent strengthening effect. This strength is significant in promoting the use of fluorescent biosensors.

This work was supported by the National Natural Science Foundation of China (Nos. 61575168 and 61265009) and the Xinjiang Science and Technology Project (No. 201412112).

References

1. J. Lu, P. S. E. Yeo, C. K. Gan, P. Wu, and K. P. Loh, Nat. Nanotechnol. **6**, 247 (2011).
2. J. H. Moon, J. H. An, U. Sim, S. P. Cho, J. H. Kang, C. Chung, J. H. Seo, J. H. Lee, K. T. Nam, and B. H. Hong, Adv. Mater. **26**, 3501 (2014).
3. X. Yan, X. Cui, and L. S. Li, J. Am. Chem. Soc. **132**, 5944 (2010).
4. J. Peng, W. Gao, B. K. Gupta, Z. Liu, R. Romero-Aburto, L. Ge, and P. M. Ajayan, Nano. Lett. **12**, 844 (2012).
5. S. H. Lin, D. H. Kim, G. H. Jun, S. H. Hong, and S. Jeon, ACS Nano. **7**, 1239 (2013).
6. M. L. Mueller, X. Yan, J. A. McGuire, and L. Li, Nano. Lett. **10**, 2679 (2010).
7. Y. Q. Dong, H. C. Pang, H. B. Yang, C. X. Guo, J. W. Shao, Y. W. Chi, C. M. Li, and T. Yu, Angew. Chem., Int. Ed. **52**, 7800 (2013).
8. S. N. Baker and G. A. Baker, Angew. Chem., Int. Ed. **49**, 6726 (2010).
9. Y. Li, Y. Zhao, H. Cheng, Y. Hu, G. Shi, L. Dai, and L. Qu, J. Am. Chem. Soc. **134**, 15 (2011).
10. X. Yan, B. Li, X. Cui, Q. Wei, K. Tajima, and L. Li, J. Phys. Chem. Lett. **2**, 1119 (2011).
11. A. K. Geim and K. S. Novoselov, Nat. Mater. **6**, 183 (2007).
12. S. S. Chou, M. De, J. Luo, V. M. Rotello, J. Huang, and V. P. Dravid, J. Am. Chem. Soc. **134**, 16725 (2012).
13. W. S. Hummers and R. E. Offeman, J. Am. Chem. Soc. **80**, 1339 (1958).
14. Z. Fan, R. Kanchanapally, and P. C. Ray, J. Phys. Chem. Lett. **4**, 3813 (2013).
15. A. Pramanik, S. R. Chavva, Z. Fan, S. Sinha, B. P. Nellore, and P. C. Ray, J. Phys. Chem. Lett. **5**, 2150 (2014).
16. A. Pramanik, Z. Fan, S. C. Reddy, S. S. Sinha, and P. C. Ray, Sci. Rep. **4**, 6090 (2014).
17. P. V. Kamat, J. Phys. Chem. Lett. **1**, 520 (2014).
18. Z. Fan, B. Yust, B. O. V. Nellore, S. S. Sinha, R. Kanchanapally, R. A. Crouch, A. Pramanik, S. C. Reddy, D. Sardar, and P. C. Ray, J. Phys. Chem. Lett. **5**, 3216 (2014).
19. D. Pan, J. Zhang, Z. Li, and M. Wu, Adv. Mater. **22**, 734 (2010).
20. L. E. Zhohravi and M. Mahmoudi, Chin. Opt. Lett. **12**, 042601 (2014).
21. T. H. Xiao, L. Gan, and Z. Y. Li, Photon. Res. **3**, 300 (2015).
22. L. A. Ponomarenko, F. Schedin, M. I. Katsnelson, R. Yang, E. W. Hill, K. S. Novoselov, and A. K. Geim, Science **320**, 356 (2008).
23. Z. P. Zhang, J. Zhang, N. Chen, and L. T. Qu, Science **5**, 58869 (2012).
24. S. J. Zhu, S. J. Tang, J. H. Zhang, and B. Yang, Chem. Commun. **48**, 4527 (2012).
25. Y. Shi, A. Pramanik, and C. Tchouwou, ACS Appl. Mater. Interfaces **7**, 10935 (2015).
26. J. Li, X. Zhang, F. Shi, Y. Xu, P. Wang, X. Yu, and J. Xu, Chin. Opt. Lett. **9**, 062901 (2011).
27. T. Jiang, J. Mo, X. Lu, P. Yan, Z. Jia, J. Li, and F. Zhang, Chin. Opt. Lett. **9**, 022801 (2011).
28. H. J. Kim, Y. Y. Kim, K. W. Lee, and S. H. Park, Sensors Ac-tuators B **155**, 673e678 (2011).
29. G. Rong, A. Najmaie, J. E. Sipe, and S. M. Weiss, Biosens. Bioelectron. **23**, 1572 (2008).
30. S. Li, J. Huang, and L. Cai, Nanotechnol. **22**, 425502 (2011).
31. G. Gaur, D. Koktysh, and S. M. Weiss, SPIE **8594**, 859401 (2013).
32. G. Gaur, D. Koktysh, and S. M. Weiss, Adv. Funct. Mater **23**, 3604 (2013).
33. H. Qiao, B. Guan, T. Böcking, M. Gal, J. J. Gooding, and P. J. Reece, Appl. Phys. Lett. **96**, 161106 (2010).
34. C. Liu, Z. Jia, and X. Lv, Phys. B Lett. **457**, 263 (2015).
35. I. Rea, L. Sansone, and M. Terracciano, Phys. Chem. C **118**, 27301 (2014).